A Novel Fidelity Based on the Adaptive Domain for Pansharpening

Jin-Liang Xiao
Joint work with *Ting-Zhu Huang**, *Liang-Jian Deng**, and *Ting Xu*

University of Electronic Science and Technology of China (UESTC)
Chengdu, Sichuan, China

July 10, 2024

Outline

Introduction: Pansharpening

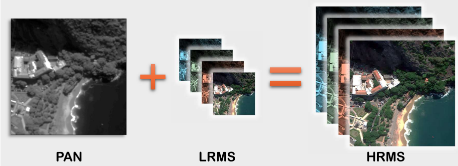

- **Goal:** obtain the high resolution multispectral image (HRMS)
- **Inputs:** the panchromatic image (PAN) and low spatial resolution multispectral image (LRMS).

- $\mathcal{X} \in \mathbb{R}^{H \times W \times S}$: HRMS;
- $\mathcal{Y} \in \mathbb{R}^{h \times w \times S}$: LRMS;
- $\mathbf{P} \in \mathbb{R}^{H \times W}$: PAN.

Variational Optimization (VO) methods

- **Variational Model:**

$$\min_{\mathcal{X}} f_{spec}(\mathcal{X}, \mathcal{Y}) + \lambda_1 f_{spa}(\mathcal{X}, \mathbf{P}) + \lambda_2 \Psi(\mathcal{X}),$$

where λ_1 and λ_2 are balance hyperparameters.

- f_{spec}: spectral fidelity

$$f_{spec} = \left\| \mathbf{X}_{(3)} \mathbf{BS} - \mathbf{Y}_{(3)} \right\|_F^2, \quad (1)$$

where $\|\cdot\|_F$ is Frobenius norm, $\mathbf{B} \in \mathbb{R}^{HW \times HW}$ and $\mathbf{S} \in \mathbb{R}^{HW \times hw}$ denote the spatial blurring matrix and down-sampling operator, respectively.

- f_{spa}: spatial fidelity is critical for spatial information extraction.
- Ψ: regularization term

Variational Optimization (VO) methods

$$\min_{\mathcal{X}} f_{spe}(\mathcal{X}, \mathcal{Y}) + \lambda_1 f_{spa}(\mathcal{X}, \mathbf{P}) + \lambda_2 \Psi(\mathcal{X}),$$

- **Spatial Fidelity f_{spa}:**

  There exists strong similarity between $\mathcal{X}$ and histogram-matched $\mathcal{P}$ [1, 2]

- [Fu *et al.* 2019]:

$$f_{spa} = \|\nabla\mathcal{X} - \nabla\mathcal{P}\|_F^2,$$

  where ∇ is the gradient operation.

- [Wu *et al.* 2024]:

$$f_{spa} = \|\mathcal{H}(\mathcal{X}) - \mathcal{H}(\mathcal{P}) + \epsilon\|_F^2,$$

  where $\mathcal{H}(\cdot)$ is the Framelet transformation, and ϵ is a sparse variable.

- ...

The above transformations are fixed.

Variational Optimization (VO) methods

$$\min_{\mathcal{X}} f_{spe}(\mathcal{X}, \mathcal{Y}) + \lambda_1 f_{spa}(\mathcal{X}, \mathbf{P}) + \lambda_2 \Psi(\mathcal{X}),$$

- **Motivation:**

- The above transformation should be more flexible;
- The extended PAN $\mathcal{P}$ should be more accurate for HRMS $\mathcal{X}$;
- Contrain the residual between the HRMS and PAN well.

The Proposed Spatial Fidelity

- **Notation $\triangle$:**

For $\mathcal{A} \in \mathbb{R}^{H\times W\times S}$, $\mathcal{A} = \mathcal{M} \triangle \mathcal{N}$ means $\mathbf{A}^{(i)} = \mathbf{M}^{(i)}\mathbf{N}^{(i)}$, $i = 1, 2, \cdots, S$.

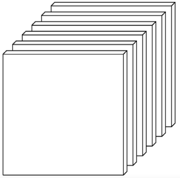

Figure: Slices of a 3rd-order tensor [3].

- **Adaptive Domain Fidelity:**

$$f_{spa} = \left\| \mathcal{W} \triangle \mathcal{X} - \mathcal{W} \triangle \mathcal{P} \right\|_0 ,$$

where $\|\cdot\|_0$ is the ℓ_0-norm, $\mathcal{P}$ is iteratively updated, and $\mathcal{W}(\cdot)$ is the Adaptive transformation that satisfies $\mathbf{W}^{(i)^T}\mathbf{W}^{(i)} = \mathbf{I}, i = 1, \cdots, S$, and r is a fixed parameter of the transform.

- **Motivation:**
  - The above transformation should be more flexible $\rightarrow$ adaptive updated transformation W
  - The extended PAN $\mathcal{P}$ should be more accurate for HRMS $\mathcal{X}$ $\rightarrow$ revise $\mathcal{P}$ iteratively
  - Constrain the residual between the HRMS and PAN well $\rightarrow$ ℓ_0-norm constraint

The Proposed Model

$$\min_{\mathcal{X}} \left\| \mathbf{X}_{(3)}\mathbf{BS} - \mathbf{Y}_{(3)} \right\|_F^2 + \lambda \left\| \mathcal{W} \triangle \mathcal{X} - \mathcal{W} \triangle \mathcal{P} \right\|_0 , \tag{2}$$

We use the ADMM [4] to solve the proposed model (2). By introducing auxiliary variables $\mathbf{U} = \mathbf{X}_{(3)}\mathbf{B}$ and $\mathcal{V} = \mathcal{W} \triangle \mathcal{X} - \mathcal{W} \triangle \mathcal{P}$, the augmented Lagrangian function concerning (2) is

$$\begin{aligned} \mathrm{L} = & \left\| \mathbf{US} - \mathbf{Y}_{(3)} \right\|_F^2 + \frac{\eta_1}{2} \left\| \mathbf{X}_{(3)}\mathbf{B} - \mathbf{U} + \frac{\mathbf{G}_1}{\eta_1} \right\|_F^2 \\ & + \frac{\eta_2}{2} \left\| \mathcal{W} \triangle \mathcal{X} - \mathcal{W} \triangle \mathcal{P} - \mathcal{V} + \frac{\mathcal{G}_2}{\eta_2} \right\|_F^2 + \lambda \left\| \mathcal{V} \right\|_0 , \end{aligned} \tag{3}$$

where η_1 and η_2 are parameters, $\mathbf{G}_1 \in \mathbb{R}^{S \times HW}$ and $\mathcal{G}_2 \in \mathbb{R}^{r \times W \times S}$ are Lagrangian multipliers.

- $\mathcal{W}$ **Sub-problem:**

$$\mathcal{W}^{k+1} = \arg\min_{\mathcal{W}} \left\| \mathcal{W} \triangle (\mathcal{X}^{k+1} - \mathcal{P}^{k+1}) - \mathcal{V}^{k+1} + \frac{\mathcal{G}_2^{k+1}}{\eta_2} \right\|_F^2 + \frac{\rho}{2} \left\| \mathcal{W} - \mathcal{W}^k \right\|_F^2 . \quad (4)$$

Since ${\mathbf{W}^{(i)}}^T \mathbf{W}^{(i)} = \mathbf{I}$, $i = 1, \cdots, S$, we have

$$(\mathbf{W}^k)^{(i)} = \mathbf{E}^{(i)} {\mathbf{F}^{(i)}}^T, i = 1, \cdots, S, \quad (5)$$

where $\mathbf{E}^{(i)} \mathbf{\Sigma}^{(i)} (\mathbf{F}^{(i)})^T$ is the singular value decomposition of $(\mathbf{V}^{k+1} - \frac{\mathbf{G}_2^{k+1}}{\eta_2})^{(i)}((\mathbf{X}^{k+1} - \mathbf{P}^{k+1})^{(i)})^T + \rho(\mathbf{W}^k)^{(i)}$ (refer to [5]).

Solving Algorithm

- **$\mathcal{V}$ Sub-problem:**

$$\mathcal{V}^{k+1} = \arg\min_{\mathcal{V}} \lambda \|\mathcal{V}\|_0 + \frac{\eta_2}{2} \left\| \mathcal{W}^k \triangle \mathcal{X}^{k+1} - \mathcal{W}^k \triangle \mathcal{P}^k - \mathcal{V} + \frac{\mathcal{G}_2^k}{\eta_2} \right\|_F^2 . \tag{6}$$

The solution of $\mathcal{V}^{k+1}$ is obtained by a classic iterative method (please refer to [6])

- **Revision of $\mathcal{P}$:**

$$\mathbf{P}_{(3)}^{k+1} = \mathbf{H}\mathbf{P}_{(3)}^{k}, \tag{7}$$

where $\mathbf{H}$ is obtained by

$$\mathbf{H} = \arg\min_{\mathbf{H}} \left\| \mathbf{X}_{(3)}^{k+1} - \mathbf{H}\mathbf{P}_{(3)}^{k} \right\|_F^2 . \tag{8}$$

Solving Algorithm

$$
\begin{cases}
\mathcal{X}^{k+1} = \arg\min_{\mathcal{X}} \frac{\eta_1}{2} \left\| \mathbf{X}_{(3)}\mathbf{B} - \mathbf{U}^k + \frac{\mathbf{G}_1^k}{\eta_1} \right\|_F^2 \\
\qquad + \frac{\eta_2}{2} \left\| \mathcal{W}^k \triangle \mathcal{X} - \mathcal{W}^k \triangle \mathcal{P}^k - \mathcal{V}^k + \frac{\mathcal{G}_2^k}{\eta_2} \right\|_F^2, \\
\mathcal{V}^{k+1} = \arg\min_{\mathcal{V}} \lambda \left\| \mathcal{V} \right\|_0 \\
\qquad + \frac{\eta_2}{2} \left\| \mathcal{W}^k \triangle \mathcal{X}^{k+1} - \mathcal{W}^k \triangle \mathcal{P}^k - \mathcal{V} + \frac{\mathcal{G}_2^k}{\eta_2} \right\|_F^2, \\
\mathbf{U}^{k+1} = \arg\min_{\mathbf{U}} \left\| \mathbf{U}\mathbf{S} - \mathbf{Y}_{(3)} \right\|_F^2 + \frac{\eta_1}{2} \left\| \mathbf{X}_{(3)}^{k+1}\mathbf{B} - \mathbf{U} + \frac{\mathbf{G}_1^k}{\eta_1} \right\|_F^2, \\
\mathbf{G}_1^{k+1} = \mathbf{G}_1^k + \eta_1 (\mathbf{X}_{(3)}^{k+1}\mathbf{B} - \mathbf{U}^{k+1}), \\
\mathcal{G}_2^{k+1} = \mathcal{G}_2^k + \eta_2 (\mathcal{W}^k \triangle \mathcal{X}^{k+1} - \mathcal{W}^k \triangle \mathcal{P}^k - \mathcal{V}^{k+1}), \\
\mathbf{P}_{(3)}^{k+1} = \mathbf{H}\mathbf{P}_{(3)}^k, \\
\mathcal{W}^{k+1} = \arg\min_{\mathcal{W}} \left\| \mathcal{W} \triangle \mathcal{T}^{k+1} - \mathcal{V}^{k+1} + \frac{\mathcal{G}_2^{k+1}}{\eta_2} \right\|_F^2 + \frac{\rho}{2} \left\| \mathcal{W} - \mathcal{W}^k \right\|_F^2,
\end{cases}
\tag{9}
$$

- **Visual Comparison on Reduced-resolution Dataset**

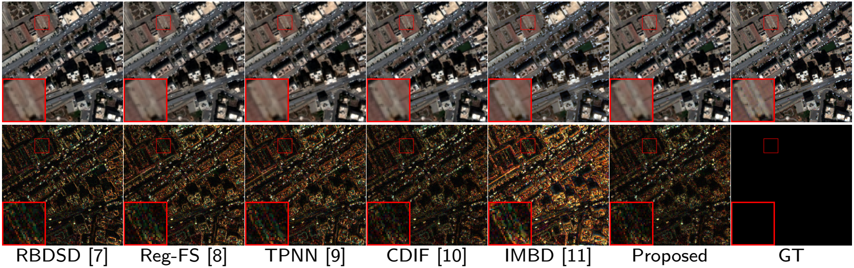

Figure: Top: Color images consisting of the 5th (R), 3rd (G), and 2nd (B) bands of the fused Tripoli dataset (reduced resolution), generated by compared methods. Bottom: The corresponding error images, enhanced by multiplying by a fixed number (i.e., 8).

- **Quantitative Comparison on Reduced-resolution Dataset**

Table: Quantitative results for 42 images from Tripoli dataset. (Bold: best; Underline: second best)

Method	PSNR ↑	SSIM ↑	SAM ↓	SCC ↑	ERGAS ↓	Q8 ↑
RBDSD [7]	31.38 ± 1.66	0.889 ± 0.07	4.335 ± 1.74	0.939 ± 0.06	3.376 ± 1.49	0.897 ± 0.11
Reg-FS [8]	30.90 ± 1.63	0.876 ± 0.07	4.345 ± 1.72	0.936 ± 0.06	3.541 ± 1.45	0.886 ± 0.11
TPNN [9]	29.30 ± 1.52	0.848 ± 0.07	5.094 ± 1.68	0.925 ± 0.05	4.197 ± 1.32	0.865 ± 0.11
CDIF [10]	<u>31.90 ± 1.57</u>	<u>0.890 ± 0.07</u>	<u>4.049 ± 1.72</u>	<u>0.946 ± 0.05</u>	<u>3.168 ± 1.41</u>	<u>0.904 ± 0.10</u>
IMBD [11]	30.13 ± 1.81	0.862 ± 0.06	4.714 ± 1.71	0.930 ± 0.06	3.845 ± 1.45	0.877 ± 0.09
Proposed	**32.13 ± 1.67**	**0.896 ± 0.06**	**3.972 ± 1.77**	**0.948 ± 0.05**	**3.094 ± 1.42**	**0.910 ± 0.10**

- **Visual Comparison on Full-resolution Dataset**

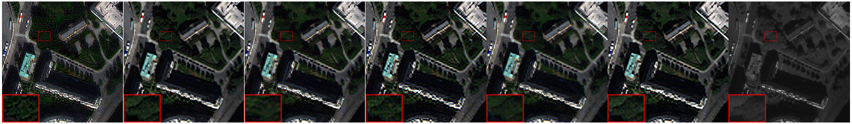

RBDSD [7] Reg-FS [8] TPNN [9] CDIF [10] IMBD [11] Proposed PAN

Figure: Color images consisting of the 5th (R), 3rd (G), and 2nd (B) bands of the Stockholm dataset (full resolution), generated by compared methods.

Full-resolution Data

- **Quantitative Comparison on Full-resolution Dataset**

Table: Quantitative results for 8 images from Stockholm dataset. (Bold: best; Underline: second best)

Method	**D_λ ↓**	**D_s ↓**	**QNR ↑**	**Runtime (s) ↓**
RBDSD [7]	<u>0.026 ± 0.009</u>	0.042 ± 0.011	0.933 ± 0.015	**0.113 ± 0.071**
Reg-FS [8]	0.059 ± 0.015	0.058 ± 0.016	0.887 ± 0.028	<u>0.114 ± 0.008</u>
TPNN [9]	0.033 ± 0.009	**0.029 ± 0.010**	<u>0.939 ± 0.012</u>	2.469 ± 0.483
CDIF [10]	0.034 ± 0.004	0.060 ± 0.010	0.908 ± 0.012	55.31 ± 0.740
IMBD [11]	**0.019 ± 0.002**	0.061 ± 0.013	0.922 ± 0.014	1.356 ± 0.014
Proposed	0.030 ± 0.007	<u>0.031 ± 0.007</u>	**0.940 ± 0.007**	24.18 ± 0.062

Reference

[1] L. Alparone, A. Garzelli, and G. Vivone. "Intersensor statistical matching for pansharpening: Theoretical issues and practical solutions". In: *IEEE Trans. Geosci. Remote Sens.* 55.8 (2017), pp. 4682–4695.

[2] X. Fu et al. "A variational pan-sharpening with local gradient constraints". In: *IEEE/CVF Conf. Comput. Vis. Pattern Recognit.* 2019, pp. 10265–10274.

[3] T. G. Kolda and B. W. Bader. "Tensor decompositions and applications". In: *SIAM rev.* 51.3 (2009), pp. 455–500.

[4] S. Boyd et al. "Distributed Optimization and Statistical Learning via the Alternating Direction Method of Multipliers". In: *Mach. Learn.* 3.1 (2011), pp. 1–122.

[5] T. Xu et al. "An iterative regularization method based on tensor subspace representation for hyperspectral image super-resolution". In: *IEEE Trans. Geosci. Remote Sens.* 60 (2022), pp. 1–16.

[6] G. Yuan and B. Ghanem. "ℓ_0TV: A Sparse Optimization Method for Impulse Noise Image Restoration". In: *IEEE Trans. Pattern Anal. Mach. Intell.* 41.2 (2019), pp. 352–364.

[7] G. Vivone. "Robust band-dependent spatial-detail approaches for panchromatic sharpening". In: *IEEE Trans. Geosci. Remote Sens.* 57.9 (2019), pp. 6421–6433.

[8] G. Vivone, R. Restaino, and J. Chanussot. "Full scale regression-based injection coefficients for panchromatic sharpening". In: *IEEE Trans. Image Process.* 27.7 (2018), pp. 3418–3431.

[9] G. Scarpa, S. Vitale, and D. Cozzolino. "Target-adaptive CNN-based pansharpening". In: *IEEE Trans. Geosci. Remote Sens.* 56.9 (2018), pp. 5443–5457.

[10] J.-L. Xiao et al. "A New Context-Aware Details Injection Fidelity with Adaptive Coefficients Estimation for Variational Pansharpening". In: *IEEE Trans. Geosci. Remote Sens.* 60 (2022), pp. 1–15.

Reference (cont.)

[11] H. Lu et al. "Intensity mixture and band-adaptive detail fusion for pansharpening". In: *Pattern Recognit.* 139 (2023), p. 109434.

My homepage

Team homepage

Thank you very much!